

# Redshifts For 220 BATSE Gamma-Ray Bursts Determined by Variability and the Cosmological Consequences

E. E. Fenimore<sup>1</sup>, and E. Ramirez-Ruiz<sup>1,2</sup>

<sup>1</sup>MS D436, Los Alamos National Laboratory, Los Alamos, NM 87545

<sup>2</sup>Institute of Astronomy, University of Cambridge, Cambridge, CB3 0HA United Kingdom

## ABSTRACT

We show that the time variability of a gamma-ray burst (GRB) appears to be correlated with the absolute luminosity of the burst: smooth bursts are intrinsically less luminous. This Cepheid-like relationship can be used to determine the redshift of a GRB from parameters measured solely at gamma-ray energies. The relationship is based on only seven events at present and needs to be further confirmed with more events. We present the details of converting GRB observables to luminosities and redshifts for 220 bright, long GRBs from the Burst and Transient Source Experiment (BATSE) and explore the cosmological consequences. In particular, we derive the GRB rate as a function of  $z$  without assuming either a luminosity function or that the GRB rate follows the star formation rate (SFR). We find that the GRB formation rate scales as  $(1+z)^{3.3\pm 0.3}$ . The observations used to derive the SFR can be strongly affected by dust for  $z \gtrsim 2$  whereas GRB observations are not. If GRBs trace star formation, then our results indicate that the SFR does not peak at  $z \sim 2$  but instead continues to increase until  $z \sim 10$ . We have used the burst formation rate to correct the observed GRB luminosity function for the incompleteness due to the detection threshold, resulting in a luminosity function with a power law index of  $\sim -2.3$  that slightly rolls over at low luminosities. The reality of our variability–luminosity relationship requires confirmation but, if valid, will provide a powerful tool for studying both GRBs and the early universe.

*Subject headings:* gamma-rays: bursts – stars: formation – cosmology: theory – large-scale structure of the universe

## 1. INTRODUCTION

Thousands of gamma-ray bursts (GRBs) have been observed, but there is no consensus on the physics underlying their defining characteristics: huge luminosity, chaotic time history, and an

energy release that peaks in the gamma-ray energy range. The Italian–Dutch BeppoSax satellite provided a crucial breakthrough in 1997 with the discovery of precisely located X-ray afterglows (Costa et al. 1997) and, subsequently, afterglows across the spectrum from optical (van Paradijs et al. 1997) to radio (Frail et al. 1997). See Kulkarni et al. 2000 for a review. The optical afterglows led to measured redshifts for a few afterglows and host galaxies, firmly establishing that GRBs are cosmological in nature and the largest explosions since the Big Bang. These few measured distances can be used to calibrate other properties of GRBs that might serve as standard candles.

The peak flux, fluence, duration, spectral hardness, and number of peaks in a GRB are clearly not standard candles. However, other properties of the time structure may be correlated with absolute luminosity. Based on an analysis of the time structure of BATSE bursts, Stern, Poutanen, & Svensson (1997, 1999) concluded that there was an intrinsic correlation between luminosity and the complexity of GRBs. Norris et al. (1999, 2000) suggested that the lag found from the cross-correlation of two spectral channels might be correlated with luminosity. Ramirez-Ruiz & Fenimore (1999) suggested that the spikiness of the time structure is correlated with luminosity, a relationship similar to the Cepheid period–luminosity relationship, in which the pulsation period of a star is correlated with luminosity. In our relationship, which is purely empirical, smooth bursts are intrinsically less luminous. We define spikiness as effectively the mean-square of the time signal after removing low frequencies by smoothing.

In this paper, we present the details of calculating quantitative values for the spikiness and its correlation with absolute luminosity. We use seven Burst and Transient Source Experiment (BATSE) GRB events for which redshifts are known to calibrate the variability – luminosity relationship. We apply the relationship to the bright, long GRBs in the BATSE catalog to obtain distances and luminosities. Based on only seven events, the variability – luminosity relationship requires more GRBs with redshifts to confirm its validity. We investigate some of the implications of the relationship, in particular, the resulting GRB luminosity function and the rate of formation of GRB progenitors.

## 2. THE VARIABILITY – LUMINOSITY RELATIONSHIP

We call the spikiness “variability” and calibrate it using GRBs with known redshifts ( $z$ ) and BATSE time histories. We must first correct the observed time history for cosmological time dilation, correcting it to how it would appear at some baseline redshift,  $z_b$ . The most natural  $z_b$  is, of course, zero. Other classes of objects, such as supernovae, have most observed events at low redshifts, which can be used to calibrate standard candles at  $z_b = 0$ . In the case of GRBs, all of the events are at quite high redshifts. The advantage of setting  $z_b$  to, say, 2 is that smaller, and thus more stable, time dilation corrections will be applied. We define  $Y$  to be  $(1 + z)/(1 + z_b)$  and we will use  $z_b = 2$  to correct the time histories for time dilation. (In previous versions of this paper we also scaled the luminosity to what it would appear to be from  $z = z_b$ . We no longer do that.)

The amount of stretching of the time history depends on  $Y$  in two ways. First, time dilation causes a stretching equal to  $Y$ . Second, the spectrum is redshifted such that the bandpass of BATSE records energies from  $YE_L$  to  $YE_U$  rather than from  $E_L$  to  $E_U$ , where  $E_L$  to  $E_U$  is the energy range of the BATSE time history. Bursts have a narrower time structure at higher energies (Fenimore et al. 1995), which affects the variability. Let  $V(E_L, E_U)$  be the variability of the GRB time structure in the bandpass  $E_L$  to  $E_U$ . The energy-dependent correction is  $V(YE_L, YE_U)/V(E_L, E_U)$ . We can estimate  $V(YE_L, YE_U)/V(E_L, E_U)$  for  $Y = 2$  because BATSE provides us with two energy channels that happen to be shifted by a factor of 2 (i.e., channel 1 [25 to 50 keV] and channel 2 [50 to 100 keV]). We selected 118 BATSE bursts that were bright (peak flux greater than  $1.5 \text{ photons s}^{-1} \text{ cm}^{-2}$ ), long (90% of the counts spread out over more than 20 s), with at least 100 points  $5\sigma$  above the background. We calculated the variability for both channel 1 and channel 2 and determined that the median  $V(YE_L, YE_U)/V(E_L, E_U)$  was  $\sim 0.85$ . Furthermore, from symmetry, we know that  $V(Y^{-1}E_L, Y^{-1}E_U)/V(E_L, E_U) \sim V(E_L, E_U)/V(YE_L, YE_U)$ , thus channel 1 and channel 2 also gives us the correction for  $Y = 0.5$  (i.e.,  $1/0.85$ ). We have little knowledge of  $V(YE_L, YE_U)/V(E_L, E_U)$  for other values of  $Y$ , but we do have the robust result that the average pulse width of a GRB as a function of energy is a power law (Fenimore et al. 1995). Thus, we assume that the correction to variability for the pulse spreading with energy is also a power law:

$$V(YE_L, YE_U)/V(E_L, E_U) = Y^{-0.24} \quad . \quad (1)$$

We have most confidence when  $Y$  is less than 2 because we can use channels 1 and 2 of BATSE to estimate the correction. If one uses  $z_b = 0$ , we could only confidently correct the energy dependency for events from  $z = 0$  to  $z = 1$ . Using  $z_b = 2$  means that we can correct with high confidence the energy dependency for events from  $z = 0.5$  to  $z = 5$ .

To calculate the variability, we first fit a linear or quadratic polynomial to the background in the non-burst portions of the data. Let  $g_i$  be the gross counts observed in a 64 ms sample in the BATSE four channel data (i.e., DISSC data, covering 25 to  $\sim 800$  keV). Let  $b_i$  be the counts in a 64 ms background sample from the polynomial fit. The net count is  $c_i = g_i - b_i$ . Using the known redshift, we correct for time dilation by rebinning the counts by stretching the time samples by  $Y$ . Let  $C_i$  be the new stretched net count. Thus,  $C_i$ , represent what the time history would look like at  $z = z_b$ . Let  $B_i$  be the stretched background. The variability is then defined to be the (energy-corrected) average mean-square of the variations in  $C_i$  relative to a smoothed time history, that is,

$$V = Y^{-0.24} \frac{1}{N} \sum \frac{(C_i - \langle C \rangle_{0.3T_{90}})^2 - (B_i + C_i)}{C_p^2} \quad (2)$$

where  $C_p$  is the peak of the (stretched) net count during the burst, and  $\langle C \rangle_{0.3T_{90}}$  is the count smoothed with a boxcar window with a length equal to 30% of the (stretched)  $T_{90}$  duration of the burst. ( $T_{90}$  is the period that contains 90% of the total counts.) The  $Y^{-0.24}$  term corrects the variability for the energy-dependence of the time scale of a GRB. The  $B_i + C_i$  term (stretched gross counts in a sample) accounts for the Poisson noise (Reichart et al. 2000). The expected value

of  $V$  for pure noise is zero. The sum is taken over the  $N$  samples that exceed the background by at least  $5\sigma$ .

In Table 1, we list the BATSE GRBs with known redshifts and the variability found using equation (2).

The associated luminosity of a GRB can be found from the redshift, the observed spectral shape, and the observed peak photon flux averaged over 256 ms in a specified energy range,  $E_{L,P}$  to  $E_{U,P}$  (i.e.,  $P_{256}$  photons  $s^{-1} \text{ cm}^{-2}$  in the 50 to 300 keV band). The peak luminosity (also averaged over 256 ms and over the same energy range) per steradian is

$$\frac{L_{256}}{d\Omega} = P_{256} \langle E \rangle D^2 \quad (3)$$

where  $D$  is the comoving distance and  $\langle E \rangle$  is the average photon energy in the luminosity bandpass per photon in the count bandpass. The comoving distance is

$$D = \int_0^z \left(\frac{c}{H_0}\right) \frac{dz}{\sqrt{\Omega_\Lambda + \Omega_m(1+z)^3}} \quad (4)$$

in which we assume  $\Omega_\Lambda = 0.7, \Omega_m = 0.3$ , and  $H_0 = 65 \text{ km s}^{-1} \text{ Mpc}^{-1}$ . From the observed photon number spectrum,  $\phi(E)$ ,

$$\langle E \rangle = \frac{\int_{E_{L,P}}^{E_{U,P}} E \phi\left[\frac{E}{1+z}\right] dE}{\int_{E_L}^{E_U} \phi[E] dE} \quad (5)$$

The observed spectra,  $\phi[E]$ , are characterized by the ‘‘Band’’ function (Band et al. 1993) defined by a low-energy spectral index,  $\alpha$ , a high-energy spectral index,  $\beta$ , and the peak of the  $E^2\phi(E)$  distribution,  $E_{\text{peak}}$ .

In equation (3), we specify luminosity per steradian to emphasize that the angular extent of the GRB emission is not known. An instrument measures the flux subtended by a detector; that is, we always measure the luminosity per solid angle. Thus, our variability – luminosity relationship is independent of the (unknown) angular range that the GRB emits into. Often, the equivalent isotropic luminosity ( $L_{4\pi}$ ) is quoted neglecting the effects of beaming;  $L_{4\pi} = 4\pi L/d\Omega$ . All our conclusions remain valid if GRBs emit in a jet, but then our numerical results must be multiplied by  $d\Omega_{\text{jet}}/4\pi$ , where  $d\Omega_{\text{jet}}$  is the jet opening angle.

In Table 1, we list  $P_{256}, \alpha, \beta, E_{\text{peak}}$ , and the resulting  $L/d\Omega$  and  $V$  for each GRB. In Figure 1, we show the variability as a function of  $L/d\Omega$  for the seven BATSE events with well known redshifts. (An eighth suggested redshift, for GRB980425, will be discussed later.) The scatter in Figure 1 is much larger than we showed in a preliminary report (Ramirez-Ruiz & Fenimore 1999). Some of the additional scatter was introduced by the addition of a new event (burst 7906). A small amount is due to slight improvements in how we correct for the time dilation, but some of the differences are unexplained.

Through Monte Carlo simulations of these bursts we have determined that the uncertainty in the position of the points due to counting statistics is about the size of the plotting symbol. If a

relationship exists between absolute luminosity and variability, then it obviously has some scatter. In Figure 1 we have suggested two power laws which probably bound the power law which best describes the real distribution. The two power laws are:

$$L/d\Omega = 5.9 \times 10^{60} V^{5.8} \text{erg s}^{-1} \quad \text{and} \quad (6)$$

$$= 2.4 \times 10^{54} V^{2.2} \text{erg s}^{-1} \quad . \quad (7)$$

These curves are only to guide the eye. Reichart et al. (2000) has done a statistical analysis of the seven events used here plus some additional upper limits to find a true confidence region for the variability – luminosity relationship. More events will be required to accurately define the real distribution.

Figure 2 shows the seven bursts used above and BATSE burst 6707 (GRB980425), which has been associated with the nearby supernova, SN 1998bw. This association is controversial (Galama et al. 1999b, Woolsey et al. 1999, Kulkarni et al. 1998, Graziani, Lamb, & Masion 2000). If the association is correct, then GRB980425 was much less luminous than other GRBs (see discussion in Bloom et al. 1999). However, its variability is also much smaller, following our general trend that low variability implies low absolute luminosity. We feel that GRB980425 adds believability to our relationship in proportion to the probability that the association with SN 1998bw is true.

### 3. Comparison to Different Definition of Variability

Recently, Reichart et al. (2000) has proposed an alternative definition of variability. Both this paper and Reichart et al. (2000) relate the variability to the square of the time history after removing low frequencies by smoothing. There are three major areas where the definitions differ; (1) the time scale for smoothing, (2) the normalization to make the definition roughly independent of distance, and (3) how time dilation and intrinsic peak-spread with energy are accommodated. Reichart et al. (2000) also does precise statistics at every step and determines confidence regions for all results. The Reichart et al. (2000) definition can be heuristically expressed as

$$V_R = \frac{1}{N_E} \sum_{\Delta E_i=1}^{\Delta E_i=N_E} \frac{\sum [ \langle c_{\Delta E_i} \rangle_{(1+z)^\beta} - \langle c_{\Delta E_i} \rangle_{T_f=0.45} ]^2}{\sum [ \langle c_{\Delta E_i} \rangle_{(1+z)^\beta} ]^2} \quad (8)$$

where  $N_E$  is the number of energy channels,  $c_{\Delta E_i}$  is the counts in the  $i$ -th energy bin, and  $\langle c_{\Delta E_i} \rangle_{(1+z)^\beta}$  indicates that the counts have been smoothed by a box car function with a width of  $(1+z)^\beta$ . This formulation is only for the purpose of indicating the major differences in the definitions and the original formulation should be consulted for details. For example, this formulation omits the various terms associated with the propagation of Poisson noise and simplifies others.

The first difference is the time scale for smoothing. We use 30% of the  $T_{90}$  duration provided by the BATSE catalog. Reichart et al. (2000) defines a duration (“ $T_{f=0.45}$ ”) equal to the smallest

fraction of the burst time history that contains a fraction  $f$  of the total counts. If all bursts had time histories that monotonically increased and then decreased, then  $T_{90}$  would be equal to  $T_{f=0.90}$ . The Reichart et al. (2000) time scale reflects the total on-time that the burst is active whereas  $T_{90}$  reflects the total range of time that the burst is active. Bursts with precursors might have a large  $T_{90}$  but a small  $T_{f=0.90}$ . Reichart et al. (2000) finds that  $f = 0.45$  gives a robust definition of variability. It is too early to tell if this different way of setting the smoothing time scale is important.

The second difference is in the normalization in the denominator. We use the square of the peak counts ( $C_p^2$ ) whereas Reichart et al. (2000) uses the sum of the counts squared. Note, that the Reichart et al. (2000) normalization is not the square of the fluence (which would be  $(\sum c_i)^2$ ). We also define the variability to be an average variation per sample (note the  $1/N$  term in eq. [2]). Thus, the difference in normalization is roughly  $NC_p^2/\sum C_i^2$ . Since  $N$  will scale as the duration of the event, our variability values will be smaller. Again, it is too early to tell if this difference in normalization is important.

The key conceptual difference is how the time dilation and the peak spreading with energy is handled. This paper treats these issues separately. We use the known  $z$  to rebin the observed time history to remove the time dilation (i.e., the conversion of the observed counts,  $c_i$ , to those corrected for time dilation,  $C_i$ ). We then remove the effects of the peak spreading by the  $Y^{-0.24}$  term in equation (2). That term was derived based on how our definition of variability varied with energy in bright BATSE bursts. We mitigate these effects by correcting the time history to how it would appear at an intermediate  $z_b$  rather than  $z = 0$ . Reichart et al. (2000) applies a smoothing to the time history to account for the combined effects of time dilation and peak spreading. Time dilation uniformly stretches the whole time history by  $(1+z)^1$  and peak spreading stretches the individual peaks by  $\sim (1+z)^{-0.4}$  (Fenimore et al. 1995). Thus, in equation (8), the time history is smoothed by  $(1+z)^\beta$  where  $\beta = 0.6$ . With such smoothing, Reichart et al. (2000) finds that each energy range gives about the same variability, so the variability from multiple energy ranges are combined with a Bayesian inference formalism which is heuristically similar to a weighted average (represented by  $\frac{1}{N_E} \sum$  in eq. [8]).

There are other minor differences. In the definition of luminosity, we use  $P_{256}$  whereas Reichart et al. (2000) uses  $P_{1024}$ . Also, we use a source frame energy range of 50 to 300 keV and the measured Band parameters whereas Reichart et al. (2000) uses 100 to 1000 keV and an average spectral shape.

Figure 3 is a scatter plot of our values of variability *vs.* the Reichart et al. (2000) values. Although there are differences in how variability is defined, the two methods give highly correlated values. Apparently all three differences in the definition are required to have such a correlation. If the Reichart et al. (2000) time scale and normalization are used in equation (2), the values are much less correlated.

#### 4. DETERMINING DISTANCE FROM GRB TIME STRUCTURE

The variability – luminosity relationship allows us to determine the distance to GRBs based only on the observed time history and parameters determined from the gamma-ray observations ( $P_{256}, T_{90}, \alpha, \beta, E_{\text{peak}}$ ).

The first step in determining distance from the time structure is to assume that  $z = z_b$  and to calculate the variability,  $V$ , using equation (2). For the variability – luminosity relationship, we have used a power law lying intermediate between the two power laws shown in Figure 1:

$$\frac{L_{4\pi}}{4\pi} = L/d\Omega = 3.1 \times 10^{56} V^{3.35} \text{erg s}^{-1} . \quad (9)$$

Here, the luminosity is the peak  $\text{erg s}^{-1}$  per steradian in a specified (source frame) energy bandpass ( $E_{L,P} = 50 \text{ keV}$  to  $E_{U,P} = 300 \text{ keV}$ ), averaged over 256 ms. The peak photon flux is

$$P_{256} = \frac{3.1 \times 10^{56} V^{3.35}}{\langle E \rangle D^2} \text{ photon cm}^{-2} \text{ s}^{-1} . \quad (10)$$

We substitute equations (2, 4, 5) into equation (10), to solve for  $z$ , the only unknown. Once we obtain  $z$  (i.e.,  $Y$ ), we iterate using equation (2) to compute an improved estimate of the variability. Equation (10) is solved again and the iterative process is repeated until  $z$  converges. In 19 cases, the solution converged to a value of  $z$  larger than 12. These cases were assigned a value of  $z$  equal to 12 in the table and in the figures. In our analysis to obtain the formation rate and the luminosity function, we do not use any part of the parameter space beyond  $z = 11.5$ .

#### 5. REDSHIFTS AND LUMINOSITIES FOR 220 BATSE GRBs

The redshifts determined from GRBs events detected by the BeppoSax satellite were only obtained for long bursts, so our luminosity – variability relationship may only be valid for long bursts. Also, variability is more difficult to estimate for short bursts. Thus, we estimate redshifts only for long ( $T_{90} > 20 \text{ s}$ ), bright ( $P_{256} > 1.5 \text{ photons s}^{-1} \text{ cm}^{-2}$ ) BATSE bursts. There are 227 such bursts in the BATSE 4B catalog (Paciesas et al. 1999). Four did not have at least 10 samples with a  $5\sigma$  significance (bursts 1145, 1546, 1626, 5572), two bursts produced negative variability (bursts 2106 and 2863), and the iterations to solve equation (10) failed for one burst (2476). These events were not considered further. We did not have “Band” parameters available, so we used the default values  $\alpha = 1.5, \beta = 2.0$ , and  $E_{\text{peak}} = 250 \text{ keV}$ .

Table 2 lists the properties of the 220 GRBs and Figure 4 shows the resulting distribution of luminosities and redshifts as open squares. The solid squares are the seven GRBs (omitting GRB980425) from Table 1. The luminosities are smaller than often quoted for GRBs because we have evaluated the luminosity assuming a finite energy range (50 to 300 keV) rather than bolometric. The solid lines are lines of constant  $P_{256}$  starting at  $P_{256} = 1.5 \text{ photon cm}^{-2} \text{ s}^{-1}$ . If we did not have a detector threshold, then the projection of the GRBs onto the luminosity

axis would directly give the GRB luminosity function. Although it is possible to imagine other scenarios, we expect the luminosity function to be the same for all redshifts. The projection of Figure 4 onto the redshift axis (divided by the volume in the redshift range 0 to  $z$ ), would give the GRB formation rate which is analogous to the star formation rate, SFR (see Madau et al. 1996). We expect every range of luminosity to have a similar GRB formation rate. The BATSE detector threshold is obviously preventing us from seeing many events at high  $z$ , as well as preventing the direct determination of the luminosity function and the burst formation rate.

Previously, we did not have estimated redshifts for so many GRBs, and so we were forced to only analyze the brightness distribution (i.e.,  $\text{Log } N\text{-Log } P_{256}$ ). All we knew was the number of GRBs between the solid lines (i.e., in ranges of  $P_{256}$ ) but not their distribution in the  $L_{4\pi} - z$  space. Hence, previous studies (e.g., Totani 1997, Wijers et al. 1998, Hogg & Fruchter 1999, Lamb & Reichart 1999) could only check for consistency between the observed distribution of  $P_{256}$  by assuming both a GRB luminosity function (usually a power law) *and* that the burst formation rate followed an assumed SFR. Indeed, we have analyzed the  $\text{Log } N\text{-Log } P_{256}$  distribution from the 220 GRBs based on the solid lines in Figure 4 and found that it gives similar results to analyses using a larger number of BATSE GRBs: the best fit power law index of the luminosity function is -2.4 and the dynamic range of the power law was a factor of 170.

The  $L_{4\pi} - z$  distribution in Figure 4 allow us to directly determine the GRB luminosity function and the burst formation without assuming that the GRB formation rate follows the SFR or assuming a form for the luminosity function.

### 5.1. Consistency with the Star Formation rate

The luminosity – redshift distribution in Figure 4 is complete at a particular redshift down to a threshold luminosity,  $L_{th}(z)$ , which follows the  $P_{256} = 1.5$  photons  $\text{cm}^{-2} \text{s}^{-1}$  line in Figure 4. We restrict ourselves to BATSE events brighter than 1.5 photons  $\text{s}^{-1} \text{cm}^{-2}$ , and so we are confident that BATSE is complete to the corresponding  $L_{256}$ . Figure 5 shows the 220 BATSE GRBs divided into ranges of  $z$  and  $L$ . Consider the dotted lines: they divide the bursts into ranges of  $z$  each selected to contain approximately the same number of events. There are seven ranges of  $z$  bound by  $z_1, z_2, \dots, z_8 = 0.3, 0.75, 1.25, 2.0, 3.0, 5.0, 7.0, 10.0$ . Within the  $i$ -th range (bounded by  $z_i$  to  $z_{i+1}$ ), the figure is complete to  $L = L_{th}(z_{i+1})$ . Within each range we can find the  $\text{Log } N\text{-Log } L_{256}$  distribution for  $L_{256} > L_{th}$  without making any corrections or assumptions. We normalize each distribution by the rate-volume between  $z_i$  and  $z_{i+1}$ , that is, we divide by

$$N_{z_i, z_{i+1}} = \int_{z_i}^{z_{i+1}} \frac{4\pi D^2 \rho(z) dz}{(1+z)\sqrt{\Omega_\Lambda + \Omega_m(1+z)^3}} \quad (11)$$

where  $\rho(z)$  is the comoving density of events. The  $1+z$  term in the denominator accounts for the fact that we observe an event rate.

In Figure 6, we show the resulting  $\text{Log } N\text{-Log } L_{256}$  distributions if the co-moving density,  $\rho(z)$ ,

is constant. The true  $\text{Log } N\text{--}\text{Log } L_{256}$  distribution is, plausibly, independent of  $z$ , whereas the distributions in Figure 6 are clearly inconsistent with each other. Of course, the likely explanation is that the density of GRBs is not constant. In Figure 7 we show the resulting  $\text{Log } N\text{--}\text{Log } L_{256}$  distributions if  $\rho(z)$  follows the SFR,  $\rho_{\text{SFR}}(z)$ , for which we have used the observations summarized by Steidel et al. 1999 as parameterized by Rowan-Robinson 1999. (Other fits to the observations including estimates of the SFR in the sub-mm waveband, such as Blain & Natarajan 1999, give similar results.) The resulting distributions are more consistent than in Figure 6, but still not consistent with each other. Clearly, bursts in  $z$ -ranges # 4, 5, 6, and 7 (i.e.,  $z > 2$ ) are occurring at a relatively higher rate than  $z$ -ranges # 1, 2, and 3 (i.e.,  $z < 2$ ).

In previous work, it was necessary to simultaneously assume that GRBs follow the SFR *and* a luminosity function, usually a bounded, power law. In that case, one could only check for consistency with the number of events found within bands such as the solid lines in Figure 4 (i.e., the  $\text{Log } N\text{--}\text{Log } P_{256}$  distribution, see Totani 1997, Wijers et al. 1998, Hogg & Fruchter 1999, Lamb & Reichart 1999). Non-evolving standard candle models would also fit (Fenimore et al., 1992, Fenimore & Bloom 1995), although the occurrence of high redshift GRBs indicated that non-evolving models were probably not acceptable (Schmidt 1999). Figure 6 demonstrates that a non-evolving, standard candle model is inconsistent with the observations. Figure 7 demonstrates for the first time that GRBs could be occurring at a higher rate than star formation at  $z > 2$ .

The normalization constants that bring the distributions of Figure 6 into agreement directly give the relative burst formation rate as a function of  $z$ . Figure 8 demonstrates this process. In Figure 8, we have shifted the curves of Figure 6 until they all fall on a common curve. The resulting factors are plotted in Figure 9 as the solid squares. The solid squares roughly follow  $(1+z)^{3.3\pm 0.3}$  and is the burst formation rate derived solely from gamma-ray data without assuming a star formation rate or a form for the luminosity function. The solid histogram uses equation (9). The dotted histograms use equations (6) and (7), so represent the systematic uncertainty in the burst formation rate from the uncertainty in the variability – luminosity relationship. The dashed line is the SFR from Blain & Natarajan 1999 that is consistent with current sub-mm observations and the solid line is from Steidel et al. 1999. The dotted curve in Figure 9 is a theoretical estimate of the star formation rate at high  $z$  (from Gnedin & Ostriker 1997). (We have arbitrarily normalized the rates to each other at  $z = 1$ .)

For  $z > 2$ , the burst formation rate is much higher than the SFR and continues to rise well beyond where other observations indicate that star formation has decreased or become constant. However, recent results indicate that the SFR may, indeed, rise until large  $z$ . The SFR may be underestimated at high redshifts ( $z > 3$ ) due to an under correction in previous surveys of cosmological surface brightness dimming. When corrected, the resulting SFR increases to  $\sim z = 10$ , similar to our result (Lanzetta, K., private communication).

If the SFR follows the burst formation rate, many more stars would have formed earlier in the universe. One can integrate the SFR based on our burst formation rate (i.e., the histogram in Fig.

[8]) from  $z = 0$  to  $\sim \infty$  to determine  $\Omega_*$ , the density parameter of stars (cf. Madau et al. 1996). We find that our burst formation rate give  $\Omega_* = 0.0062 \pm 0.0005$  whereas the density contained in the stellar population based on the observed luminous mass is believed to be  $\sim 0.0045 \pm 0.0014$  (Fukugita, Hogan, & Peebles 1998, Trentham & Poggiantiin 2000). Current Models used to obtain the SFR (such as Steidel et al. 1999) give values of  $\Omega_*$  between 0.0028 and 0.0035. Thus, current SFR predictions give values that are about  $1\sigma$  lower than those obtained from the luminous mass estimates, and our burst formation rate gives a value that is about  $1\sigma$  higher. Our burst formation rate probably reflects the formation of massive stars that become black holes whereas the SFR mostly reflect less massive stars. Thus, these two formation rates sample different parts of the mass function of stars.

GRBs are likely to provide a more robust estimate for the SFR at redshifts where the optical estimates of the SFR are affected by dust (see, for example, detailed calculations by Lamb & Reichart 1999, Blain & Natarajan 1999). However, the relationship might be complex because there could be an offset time between the star formation and the GRB phase (especially if the mechanism is neutron star – black hole collisions) and also might depend on the metallicity (see Bloom, Sigurdsson, & Pols 1999).

## 5.2. GRB Luminosity Function

The solid lines in Figure 5 divide the bursts into ranges of luminosity. There are nine ranges, spaced logarithmically. Within the  $i$ -th range (bounded by  $L_i$  to  $L_{i+1}$ ), the figure is complete to  $z_c$  defined by  $L_i = L_{th}(z_c)$ . The largest  $z_c$  is 11.5. If there were no threshold, we could count the relative number of events in each range of luminosity and determine the GRB luminosity function directly. Thus, to estimate the GRB luminosity function, we must correct for the events that are missing due to the detector threshold. For each range of luminosity, we find the number of GRBs between  $z = 0$  and  $z_c$ . We then correct that number by the relative amount of star formation for  $z < z_c$  compared to the total amount of star formation to large  $z$ . Using equation (11), we multiply the number of GRBs observed at  $z < z_c$  by  $N_{0,\infty}/N_{0,z_c}$ . The normalized number of GRBs was divided by the exposure time of the 4B BATSE catalog (2.56 yr) and by the width of the luminosity bin in units of  $10^{50}$  erg s $^{-1}$ .

The results are shown in Figure 10. The solid line uses the SFR of Steidel et al. 1999 in equation (11). The dotted line uses the GRB formation rate from Figure 9. Previously, studies had to assume a form for the luminosity function (e.g., a bounded power law) and assume that the GRB formation rate follows the SFR. Here, we have determined the GRB luminosity function without assuming a form for it or assuming that GRB follow the SFR. The dotted line is derived entirely from gamma-ray data.

Both the luminosity function based on the SFR and the luminosity function entirely from gamma-ray data are similar. Above  $L = 4 \times 10^{51}$  erg s $^{-1}$ , the luminosity function is roughly a

power law with an index of about -1.9 when using the SFR and an index of about -2.3 when using the GRB formation rate. At low luminosity, the observed distribution falls somewhat below the extensions of the power laws. Previous studies indicated that the luminosity function must be bounded (see e.g, Loredó & Wasserman 1998, Schmidt 1999, Lamb & Reichart 1999). For example, Schmidt (1999) argued that the observations of redshifts as high as 3.4 (GRB991214) requires density evolution and a broad luminosity function. Only models in Schmidt (1999) that used a luminosity function similar to our Figure 10 (i.e., a range of 3 orders of magnitude and a high luminosity slope of 2) gave reasonable probabilities for observing an event with a redshift of 3.4. Since our burst formation rate increases beyond  $z = 1$  while the SFR of Schmidt (1999) remained constant for  $z > 1$ , we would expect even higher estimates for the probability of observing events out to  $z = 3.4$ . In Figure 10 we might be seeing the gradual roll over of the distribution at low luminosity.

## 6. TIME DILATION?

Norris et al. (1994) binned BATSE bursts by  $P_{256}$  and searched for the effects of time dilation. If GRBs are standard candles, then there should be a one-to-one relationship between  $P_{256}$  and  $z$ . Bursts with smaller values of  $P_{256}$  should appear longer due to the time dilation caused by the expansion of the universe. Indeed, Norris et al. (1994) found significant time dilation by effectively binning GRBs in a manner similar to the solid lines in Figure 4. Our results clearly indicate that GRBs are not standard candles. By binning the events by  $z$  (as in Figure 5), we should be able to make a direct segregation of events by  $z$  and, therefore, see time dilation that is not smeared out by having events from different  $z$  in each sample.

We use the aligned peak test (Mitrofanov et al. 1993) to characterize the time scale in each  $z$  bin. In the aligned peak test, one shifts the time histories until the largest peaks are aligned and then an average is taken of the time histories. Figure 11 shows the aligned peaks for the first six ranges of  $z$  from Figure 5. (The seventh bin has fewer events.) All  $z$ -ranges give about the same temporal structure. The time structure is affected by the expansion of the universe in two ways. First, the expansion introduces a time dilation stretching of  $1 + z$ . Second, the time histories are redshifted by a factor of  $1 + z$  so that events at low  $z$  appear to be destretched because there is a tendency for time histories to have wider peaks at lower energy. Fenimore et al. (1995) found that the redshift effect on the aligned peak width scales as  $(1 + z)^{-0.42}$ . Thus, one would expect the aligned peak width to be stretched by  $(1 + z)^{0.58}$ . In Figure 12, we destretched each burst by a factor of  $(1 + z)^{-0.58}$  before aligning and averaging.

Since Figure 12 has been corrected for time dilation, we would expect it to have a tighter clustering of curves. Comparing Figures 11 and 12, it appears that correcting for the amount of time stretching that we expect actually makes the averaged aligned peaks more inconsistent. Thus, this test does not support that variability provides valid redshifts. This test ought to be fairly sensitive because of the wide range of  $z$  that we cover. The typical redshift in the first

range is 0.5 and the typical redshift in the sixth is 6, so one should expect nearly a factor of  $(7/1.5)^{0.58} = 2.4$  difference in the pulse widths. The test might be weak for several reasons. First, usually one needs at least 40 GRBs in each sample to average out the burst-to-burst variations. In our six samples, there are only 16, 21, 22, 25, 30, and 16 GRBs. Second, the pulse width could be an intrinsic property of the bursts that depends strongly on luminosity, and thus, less weakly on  $z$  (Lamb 1999). Perhaps with more bursts and using a lower threshold, we would be able to make a stronger test.

## 7. SUMMARY

The variability – luminosity relationship could be a powerful tool for understanding GRBs. We have presented a method for characterizing the variability of a burst (Eq. [2]) and related it to the absolute GRB luminosities. (Fig. 1). The variability – luminosity relationship (eq. 9) is based on only seven events, so its real test will come from future GRBs with known redshifts. In the interim, one can check if it produces reasonable results for the GRB luminosity function and the GRB formation rate. We have presented the details for converting the observables (i.e.,  $T_{90}$ ,  $P_{256}$ ,  $\alpha$ ,  $\beta$ ,  $E_{\text{peak}}$ , and the observed net counts) to the GRB distance using equations (2) and (10). The resulting luminosities and redshifts for 220 bright, long BATSE GRBs are shown in Table 2 and Figure 4.

The luminosity – redshift distribution allows us to find the brightness distribution (Log  $N$ –Log  $L_{256}$ ) in several ranges of  $z$ . If we assume no evolution, then the distributions are clearly inconsistent with each other (Fig. 6). Assuming reasonable SFRs improves the consistency as a function of  $z$ , but apparently the SFR underestimates the true rate of GRBs at  $z > 2$  (Fig. 7). Unlike previous work, the GRB formation rate is estimated without making any assumptions about either the luminosity function or the SFR. The resulting GRB formation rate (Fig. 9) is roughly a power law,  $\sim (1 + z)^{3.3 \pm 0.3}$ . It continues to rise at redshifts where various optical observations indicate that the SFR levels off. Unlike the SFR inferred from optical observations, the GRB formation rate is not affected by dust.

Based on a power law luminosity function and the SFR, Kommers et al. (2000) concluded from the Log  $N$ –Log  $P$  distribution that BATSE was detecting most (50% to 70%) of the GRBs that occur. Our burst formation rate implies that BATSE is seeing only a small fraction of the GRBs. Assuming a BATSE threshold of  $P_{256} = 0.5$  photons  $\text{s}^{-1} \text{cm}^{-2}$  and conservatively using a power law luminosity function (index = -1.9) that extends from  $10^{50}$  to  $10^{52.6}$  erg  $\text{s}^{-1}$ , we find that BATSE is seeing only 18% of the bursts with  $z < 2$  and only 3% of bursts with  $z < 10$ . An instrument with a threshold 5 times smaller, would see 58% of the bursts with  $z < 2$  and 11% of bursts with  $z < 10$ . Thus, such an instrument (e.g., Swift, see Gehrels et al. 2000) would see about 3 to 4 times more bursts per steradian than BATSE. With a luminosity function power law with an index of -2.3, such an instrument would see 5 times more bursts than BATSE.

We have used the GRB formation rate and the SFR to correct the observed GRB luminosity function for the incompleteness due to the detector threshold. The resulting luminosity function (Fig. 10) is a power law with an index of  $\sim -2.3$  above  $4 \times 10^{51}$  erg s $^{-1}$  and rolls over slightly at lower luminosities.

The reality of our variability – luminosity relationship is far from certain. It is based on only seven events, although GRB980425 (if associated with SN 1998bw) follows the same trend. We failed to detect the expected time dilation implied by our variability – luminosity relationship (Figs. 11 and 12), but that test is weakened by the few number of bursts that define each aligned peak average. More GRBs redshifts are needed to test whether variability or correlation lags (Norris et al. 2000) can, indeed, give redshifts to GRBs solely from gamma-ray observations.

The underlying cause of a luminosity – variability relationship is unclear. In the context of the internal shock model, larger initial Lorentz factors tend to produce more efficient collisions and, for the same number of initial shells, the time histories are more variable. (Kobayashi, Piran, & Sari 1997). We have run such models, including deceleration (c.f., Fenimore & Ramirez-Ruiz 2000), and find that simply varying the Lorentz factors, ambient density, and/or the initial mass of the shells does not produce the dynamic range of variability that is observed. Apparently, the observed luminosity – variability correlation is set deep in the center engine.

*Acknowledgments:* We recognize useful conversations and insights from A. Blain, J. Bloom, D. Lamb, J. Norris, A. Merloni, M. Rees, D. Reichart, P. Madau, and P. Natarajan. We thank D.Lamb for suggesting the term “Cepheid-like relationship”. We thank D. Reichart for pointing out the importance of subtracting the contribution from Poisson noise from the variability measure. D. Reichart and Brad Schafer pointed out serious problems in the original manuscript that caused many of the  $z$  values to be smaller.

## REFERENCES

- Band, D., et al., 1993, ApJ 413, 281.
- Blain, A. W., & Natarajan, P., 1999, submitted to MNRAS, (astro-ph/9911468)
- Bloom, J. S., Kulkarni, S. R., Harrison, F., Prince, T., Phinney, E. S. & Frail, D. A. 1998, ApJ, 506, L105
- Bloom, J. S., Sigurdsson, S., & Pols, O. P. 1999, MNRAS, 305, 763
- Costa, E., et al., 1997, Nature, 387, 783
- Djorgovski, S. G. 1998, ApJ Lett., 508, L17
- Fenimore, E. E., & Bloom, J. S. 1995, ApJ, 453, 25
- Fenimore, E. E., & Ramirez-Ruiz, E. 2000, submitted to ApJ, (astro-ph/9909299)
- Fenimore, E. E., 1992, Nature, 357, 140
- Fenimore, E. E., in't Zand, J. J., Norris, J. P., Bonnell, J. T., & Nemiroff, R. J., 1995, ApJ 448, L101
- Frail, D., Kulkarni, S. R., Nicastro, L., Feroci, M., & Taylor, G. B., 1997, Nature, 389, 261
- Fukugita, M., Hogan, C. J., & Peebles, P. J. E., 1998, ApJ, 508, 518
- Galama, T. J., et al., 1999a, Nature, 395, 670
- Galama, T. J., et al., 1999b, Astron. Astrophys. Supp. 138, 465
- Gehrels, N., et al. 2000, to appear in the Proc. of the 5th Huntsville Gamma-ray Burst Symposium.
- Gnedin, N. Y., & Ostriker, J. P. 1997, ApJ, 486, 581
- Graziani, G., Lamb, D. Q., & Masion, H., 2000, ApJ, in press (astro-ph/9810374)
- Hogg, D. W., & Fruchter, A. S., 1999, ApJ 520, 54
- Kobayashi, S., Piran, T., & Sari, R., 1997, ApJ 490, 92
- Kommers, J. M., et al., 2000, ApJ, 533, 696, astro-ph/9809300
- Kulkarni, S., et al. 1998, Nature 393, 35
- Kulkarni, S., et al. 1999, Nature 398, 389
- Kulkarni, S., et al. 2000, to appear in the Proc. of the 5th Huntsville Gamma-ray Burst Symposium (astro-ph/0002168)

- Lamb, D. Q., 1999, *A&AS*, 138, 607
- Lamb, D. Q., & Reichart, D. E. 2000, *ApJ*, in press, (astro-ph/9909002)
- Loredo, T. J., & Wasserman, I. M. 1998, *ApJ*, 502, 72
- Madau, P., et al., 1996, *MNRAS*, 283, 1388
- Metzger, M. R., et al. 1997, *Nature*, 387, 878
- Mitrofanov, I. G., et al. 1993, in *AIP Conf. Proc. 280*, Compton Gamma-Ray Observatory, ed. M. Friedlander, N. Gehrels, & D. J. Macomb (New York: AIP), 761
- Norris, J. P., et al., 1994, *ApJ* 424, 540
- Norris, J. P., et al. 1999, Presentation at the 1999 Huntsville GRB conference
- Norris, J. P., et al., 2000, *ApJ*, in press, (astro-ph/9903233)
- Odehahn, S. C., et al. 1997, *IAUC* 6753
- Paciesas, et al., 1999, *ApJ Supp.* 122, 465
- Ramirez-Ruiz, E., & Fenimore, E. E., 1999, Presentation at the 1999 Huntsville GRB conference
- Reichart, D. E., Lamb, D. Q., Fenimore, E. E., Ramirez-Ruiz, E., Cline, T. L., & Hurley, K. 2000, *ApJ*, submitted, (astro-ph/0004302)
- Rowan-Robinson, M. 1999, *Astrophys. & Space Sci*, in press, (astro-ph/9906308)
- Schmidt, M., 1999, *ApJ* 523, L117
- Steidel, C. C., et al. 1999, *ApJ*, 519, 1
- Stern, B., Poutanen, J., & Svensson, R., 1997, *ApJL*, 489, L41
- Stern, B., Poutanen, J., & Svensson, R., 1999, *ApJ*, 510, 312
- Totani, T. 1997, *ApJ*, 486, L71
- Trentham N., & Poggiantiin, B., in preparation.
- van Paradijs, J., et al. 1997, *Nature*, 386, 686
- Vreeswijk, P., et al. 1999a, *GCN Cir.* 310
- Vreeswijk, P., et al. 1999b, *GCN Cir.* 496
- Wijers, R. A. M. J., et al., 1998, *MNRAS*, 294, L13
- Woolsey, S. E., Eastman, R. G., & Schmidt, B. P. 1999, *ApJ* 516, 788

Table 1  
Burst Parameters

GRB	BATSE								
	Number	$z$	$T_{90}$	$P_{256}^1$	$\alpha^2$	$\beta^2$	$E_{peak}^2$	Variability	$L/d\Omega$
970508 <sup>3</sup>	6225	0.835	13.3	1.2	-1.18	-1.88	137.2	0.0114	$5.75 \times 10^{49}$
970828 <sup>4</sup>	6350	0.958	8.76	4.9	-0.87	-2.08	176.0	0.0173	$2.95 \times 10^{50}$
971214 <sup>5</sup>	6533	3.412	29.9	2.3	-1.14	-2.85	106.8	0.0195	$2.81 \times 10^{51}$
980425 <sup>6</sup>	6707	0.0085	20.6	1.1	-1.50	-2.00	250.0	0.0036	$2.63 \times 10^{45}$
980703 <sup>7</sup>	6891	0.967	51.2	2.6	-1.32	-2.04	181.0	0.0168	$1.82 \times 10^{50}$
990123 <sup>8</sup>	7343	1.600	63.7	16.4	-1.06	-2.30	267.7	0.0276	$2.88 \times 10^{51}$
990510 <sup>9</sup>	7560	1.62	60.6	8.2	-1.43	-2.49	74.2	0.0608	$2.57 \times 10^{51}$
991216 <sup>10</sup>	7906	1.02	40.3	85.1	-1.50	-2.00	250.0	0.0268	$6.76 \times 10^{51}$

<sup>1</sup> Peak photon flux ( $\text{ph cm}^{-2} \text{s}^{-1}$ ) on 256 ms time scale, 50 - 300 keV

<sup>2</sup> Time resolved fits from 128 channel spectral data (R. Preece, private communication)

<sup>3</sup> Metzger et al. 1997

<sup>4</sup> Odewahn et al. 1997

<sup>5</sup> Kulkarni et al. 1998

<sup>7</sup> Djorgovski 1998

<sup>6</sup> Galama et al. 1999a, default Band parameters

<sup>8</sup> Kulkarni et al. 1999

<sup>9</sup> Vreeswijk et al. 1999a

<sup>10</sup> Vreeswijk et al. 1999b

TABLE 2  
Redshifts and Luminosities of BATSE GRBs from Variability<sup>1</sup>

#	$P_{256}$	$T_{90}$	$V$	$z$	$L_{4\pi}$	#	$P_{256}$	$T_{90}$	$V$	$z$	$L_{4\pi}$
109	3.62	90.2	0.0233	1.8	$1.35 \times 10^{52}$	130	3.47	62.0	0.0168	1.1	$4.52 \times 10^{51}$
143	47.57	50.8	0.0598	2.3	$3.16 \times 10^{53}$	219	18.06	29.7	0.0172	0.6	$4.84 \times 10^{51}$
222	3.99	73.1	0.0380	3.6	$6.92 \times 10^{52}$	249	34.62	28.5	0.0170	0.4	$4.67 \times 10^{51}$
394	4.78	106.1	0.0172	1.0	$4.91 \times 10^{51}$	398	1.71	25.6	0.0175	1.6	$5.18 \times 10^{51}$
467	7.73	37.7	0.0312	2.0	$3.59 \times 10^{52}$	503	5.05	46.7	0.0753	10.2	$6.85 \times 10^{53}$
548	2.00	36.2	0.0162	1.4	$3.99 \times 10^{51}$	563	1.89	22.5	0.0115	0.9	$1.25 \times 10^{51}$
647	7.07	59.6	0.0293	1.9	$2.92 \times 10^{52}$	660	4.55	20.2	0.0305	2.4	$3.31 \times 10^{52}$
676	4.20	77.8	0.0254	1.9	$1.81 \times 10^{52}$	678	6.18	53.9	0.0226	1.4	$1.21 \times 10^{52}$
761	3.21	81.5	0.0364	3.8	$6.02 \times 10^{52}$	869	3.52	110.5	0.0557	7.3	$2.50 \times 10^{53}$
907	3.57	158.1	0.0386	3.9	$7.34 \times 10^{52}$	973	5.29	90.0	0.0462	4.3	$1.33 \times 10^{53}$
1141	9.01	20.1	0.0142	0.6	$2.55 \times 10^{51}$	1150	1.71	61.6	0.0366	5.1	$6.10 \times 10^{52}$
1157	10.04	170.6	0.0697	6.3	$5.31 \times 10^{53}$	1235	2.53	190.0	0.0854	12.0	$1.04 \times 10^{54}$
1288	6.55	318.6	0.0269	1.7	$2.18 \times 10^{52}$	1385	3.62	51.8	0.0192	1.4	$7.04 \times 10^{51}$
1396	1.68	21.0	0.0418	6.4	$9.54 \times 10^{52}$	1419	4.51	122.5	0.0642	8.2	$4.02 \times 10^{53}$
1440	11.50	24.4	0.0526	3.7	$2.06 \times 10^{53}$	1447	1.74	22.7	0.0151	1.3	$3.16 \times 10^{51}$
1467	2.26	26.8	0.0176	1.5	$5.26 \times 10^{51}$	1468	3.34	51.1	0.0519	6.6	$1.97 \times 10^{53}$
1533	4.00	99.8	0.0489	5.5	$1.62 \times 10^{53}$	1541	35.58	26.2	0.0266	0.8	$2.10 \times 10^{52}$
1578	3.75	20.5	0.0131	0.8	$1.96 \times 10^{51}$	1579	3.25	73.5	0.0614	9.0	$3.46 \times 10^{53}$
1601	2.14	48.5	0.0542	9.0	$2.28 \times 10^{53}$	1606	7.82	88.6	0.0200	1.0	$8.08 \times 10^{51}$
1623	2.98	66.1	0.0291	2.7	$2.85 \times 10^{52}$	1652	4.08	67.7	0.0244	1.8	$1.57 \times 10^{52}$
1660	1.67	53.9	0.0669	12.0	$4.61 \times 10^{53}$	1663	19.00	36.0	0.0249	1.0	$1.69 \times 10^{52}$
1676	10.49	52.8	0.0386	2.4	$7.30 \times 10^{52}$	1712	3.10	307.6	0.0341	3.4	$4.83 \times 10^{52}$
1733	3.00	36.9	0.0392	4.4	$7.70 \times 10^{52}$	1734	1.70	46.7	0.0876	12.0	$1.14 \times 10^{54}$
1819	2.01	53.0	0.1347	12.0	$4.81 \times 10^{54}$	1886	16.37	275.7	0.1072	10.3	$2.24 \times 10^{54}$
1967	1.72	25.4	0.0146	1.3	$2.80 \times 10^{51}$	1982	1.68	109.8	0.0279	3.3	$2.45 \times 10^{52}$
1989	2.73	272.4	0.0534	7.7	$2.17 \times 10^{53}$	1993	1.69	30.5	0.0371	5.3	$6.39 \times 10^{52}$
1997	16.35	60.2	0.0195	0.7	$7.46 \times 10^{51}$	2047	2.12	41.1	0.0703	12.0	$5.45 \times 10^{53}$
2061	2.19	174.7	0.0185	1.6	$6.23 \times 10^{51}$	2067	18.10	30.9	0.0132	0.4	$2.00 \times 10^{51}$
2080	5.64	53.8	0.0186	1.1	$6.39 \times 10^{51}$	2090	10.15	38.1	0.0607	4.9	$3.33 \times 10^{53}$
2122	1.89	120.6	0.0187	1.7	$6.42 \times 10^{51}$	2123	2.12	22.0	0.0032	0.1	$0.18 \times 10^{50}$
2138	7.00	77.3	0.0313	2.1	$3.61 \times 10^{52}$	2156	16.57	154.4	0.0282	1.2	$2.55 \times 10^{52}$
2190	1.82	135.9	0.0262	2.9	$2.00 \times 10^{52}$	2193	1.55	135.2	0.0219	2.4	$1.10 \times 10^{52}$
2213	4.59	61.9	0.0457	4.5	$1.29 \times 10^{53}$	2228	8.10	90.1	0.0262	1.5	$1.99 \times 10^{52}$
2232	6.02	56.5	0.0651	7.2	$4.21 \times 10^{53}$	2287	1.91	462.0	0.0337	4.2	$4.65 \times 10^{52}$
2316	3.83	29.2	0.0024	0.1	$0.64 \times 10^{49}$	2328	1.57	54.0	0.0230	2.6	$1.30 \times 10^{52}$
2329	40.40	22.1	0.0183	0.4	$5.96 \times 10^{51}$	2340	1.61	22.5	0.0490	8.8	$1.63 \times 10^{53}$
2345	2.49	89.0	0.0953	12.0	$1.51 \times 10^{54}$	2346	2.93	83.1	0.0504	6.7	$1.78 \times 10^{53}$

TABLE 2 *continued*  
 Redshifts and Luminosities of BATSE GRBs from Variability<sup>1</sup>

#	$P_{256}$	$T_{90}$	$V$	$z$	$L_{4\pi}$	#	$P_{256}$	$T_{90}$	$V$	$z$	$L_{4\pi}$
2362	3.35	45.3	0.0640	9.5	$3.97 \times 10^{53}$	2383	3.06	50.9	0.0333	3.3	$4.48 \times 10^{52}$
2387	3.86	42.0	0.0098	0.5	$7.51 \times 10^{50}$	2428	2.05	144.9	0.0617	11.6	$3.51 \times 10^{53}$
2436	6.08	33.3	0.0221	1.3	$1.13 \times 10^{52}$	2443	2.10	28.9	0.0245	2.5	$1.60 \times 10^{52}$
2450	7.57	45.9	0.0262	1.5	$1.99 \times 10^{52}$	2451	2.82	35.0	0.0487	6.5	$1.59 \times 10^{53}$
2511	1.79	64.3	0.0714	12.0	$5.74 \times 10^{53}$	2519	1.53	90.2	0.0595	12.0	$3.11 \times 10^{53}$
2522	3.23	83.1	0.0272	2.4	$2.27 \times 10^{52}$	2530	1.86	194.9	0.0323	4.0	$4.04 \times 10^{52}$
2533	8.92	74.3	0.0133	0.5	$2.06 \times 10^{51}$	2581	1.66	104.4	0.0504	9.0	$1.79 \times 10^{53}$
2593	1.56	29.9	0.0376	5.6	$6.72 \times 10^{52}$	2603	3.19	24.7	0.0082	0.4	$4.01 \times 10^{50}$
2606	2.38	134.7	0.0193	1.6	$7.15 \times 10^{51}$	2665	1.99	30.6	0.0398	5.5	$8.10 \times 10^{52}$
2681	1.64	55.5	0.0427	6.8	$1.03 \times 10^{53}$	2700	4.06	57.9	0.0371	3.4	$6.38 \times 10^{52}$
2703	2.89	57.7	0.0215	1.8	$1.02 \times 10^{52}$	2780	1.59	53.6	0.0179	1.7	$5.57 \times 10^{51}$
2790	3.47	45.3	0.0333	3.1	$4.46 \times 10^{52}$	2798	23.75	49.2	0.0230	0.8	$1.29 \times 10^{52}$
2812	10.52	30.7	0.0364	2.2	$5.99 \times 10^{52}$	2831	43.43	150.1	0.0249	0.7	$1.69 \times 10^{52}$
2855	9.53	42.5	0.0175	0.8	$5.19 \times 10^{51}$	2877	2.92	114.1	0.0356	3.8	$5.56 \times 10^{52}$
2889	5.92	75.9	0.0125	0.6	$1.68 \times 10^{51}$	2890	2.32	51.6	0.0224	2.1	$1.19 \times 10^{52}$
2891	8.71	60.7	0.0314	1.9	$3.65 \times 10^{52}$	2897	2.94	28.0	0.0178	1.3	$5.44 \times 10^{51}$
2913	5.20	22.9	0.0449	4.2	$1.22 \times 10^{53}$	2922	2.85	160.8	0.0399	4.6	$8.19 \times 10^{52}$
2929	5.91	42.8	0.0185	1.0	$6.25 \times 10^{51}$	2958	3.75	36.9	0.0406	4.2	$8.69 \times 10^{52}$
2984	4.61	32.8	0.0302	2.4	$3.21 \times 10^{52}$	2993	3.22	44.8	0.0249	2.1	$1.68 \times 10^{52}$
2994	14.42	48.6	0.0245	1.1	$1.59 \times 10^{52}$	3001	4.19	29.7	0.0337	2.9	$4.63 \times 10^{52}$
3003	2.83	37.6	0.0108	0.7	$1.02 \times 10^{51}$	3011	1.68	49.7	0.0433	6.9	$1.08 \times 10^{53}$
3015	1.75	26.8	0.0453	7.3	$1.25 \times 10^{53}$	3035	6.03	88.4	0.0198	1.1	$7.82 \times 10^{51}$
3040	1.70	26.0	0.0376	5.4	$6.69 \times 10^{52}$	3042	6.74	182.0	0.0417	3.3	$9.50 \times 10^{52}$
3055	1.78	40.6	0.0047	0.2	$0.61 \times 10^{50}$	3056	2.41	36.3	0.0196	1.7	$7.58 \times 10^{51}$
3057	32.36	34.9	0.0256	0.8	$1.84 \times 10^{52}$	3067	18.67	67.0	0.0451	2.3	$1.23 \times 10^{53}$
3075	2.32	43.6	0.0304	3.3	$3.30 \times 10^{52}$	3093	2.03	89.3	0.0431	6.2	$1.06 \times 10^{53}$
3101	2.22	37.4	0.0661	12.0	$4.43 \times 10^{53}$	3115	11.10	45.3	0.0557	4.1	$2.50 \times 10^{53}$
3128	12.41	32.2	0.0365	2.0	$6.07 \times 10^{52}$	3142	2.03	33.1	0.0424	5.9	$10.00 \times 10^{52}$
3178	14.34	39.9	0.0225	0.9	$1.20 \times 10^{52}$	3212	2.02	83.4	0.0416	5.9	$9.38 \times 10^{52}$
3227	17.03	115.3	0.0260	1.1	$1.95 \times 10^{52}$	3237	2.01	46.2	0.0582	10.3	$2.89 \times 10^{53}$
3241	12.48	45.4	0.0368	2.0	$6.25 \times 10^{52}$	3245	12.79	77.1	0.0207	0.9	$9.00 \times 10^{51}$
3255	11.87	34.9	0.0248	1.2	$1.66 \times 10^{52}$	3256	1.76	96.6	0.0965	12.0	$1.58 \times 10^{54}$
3257	3.06	63.6	0.0290	2.7	$2.81 \times 10^{52}$	3283	2.57	45.8	0.0633	10.8	$3.83 \times 10^{53}$
3287	6.69	33.4	0.0200	1.1	$8.13 \times 10^{51}$	3290	10.70	43.7	0.0803	7.6	$8.51 \times 10^{53}$
3301	2.81	36.1	0.0268	2.5	$2.17 \times 10^{52}$	3306	3.28	108.5	0.0279	2.5	$2.47 \times 10^{52}$
3307	1.70	43.0	0.0572	11.2	$2.74 \times 10^{53}$	3319	2.11	206.3	0.2210	12.0	$2.53 \times 10^{55}$
3330	6.75	62.0	0.0196	1.1	$7.58 \times 10^{51}$	3345	6.76	40.4	0.0359	2.6	$5.72 \times 10^{52}$

TABLE 2 *continued*  
 Redshifts and Luminosities of BATSE GRBs from Variability<sup>1</sup>

#	$P_{256}$	$T_{90}$	$V$	$z$	$L_{4\pi}$	#	$P_{256}$	$T_{90}$	$V$	$z$	$L_{4\pi}$
3351	4.48	102.9	0.0354	3.1	$5.50 \times 10^{52}$	3352	3.71	46.3	0.0047	0.2	$0.62 \times 10^{50}$
3405	1.53	67.4	0.0622	12.0	$3.61 \times 10^{53}$	3407	1.53	91.4	0.0435	7.3	$1.09 \times 10^{53}$
3408	12.73	58.6	0.0283	1.4	$2.59 \times 10^{52}$	3415	9.16	54.3	0.0353	2.2	$5.42 \times 10^{52}$
3436	3.56	40.0	0.0264	2.2	$2.06 \times 10^{52}$	3439	1.66	150.8	0.0933	12.0	$1.41 \times 10^{54}$
3448	2.19	331.2	0.0313	3.5	$3.64 \times 10^{52}$	3458	8.68	673.8	0.0709	6.9	$5.62 \times 10^{53}$
3481	21.94	40.8	0.0397	1.8	$8.03 \times 10^{52}$	3488	8.65	60.2	0.0521	4.2	$2.00 \times 10^{53}$
3489	6.65	33.1	0.0147	0.7	$2.89 \times 10^{51}$	3512	4.84	29.8	0.0417	3.8	$9.51 \times 10^{52}$
3523	21.57	59.1	0.0208	0.7	$9.21 \times 10^{51}$	3569	4.53	21.0	0.0832	12.0	$9.59 \times 10^{53}$
3593	6.61	59.1	0.0450	3.7	$1.23 \times 10^{53}$	3618	2.50	90.2	0.0335	3.7	$4.56 \times 10^{52}$
3634	3.30	142.0	0.0518	6.6	$1.96 \times 10^{53}$	3648	5.70	57.1	0.0297	2.1	$3.04 \times 10^{52}$
3649	4.28	26.5	0.0297	2.4	$3.02 \times 10^{52}$	3662	3.05	68.9	0.0503	6.5	$1.77 \times 10^{53}$
3663	4.48	204.4	0.0452	4.5	$1.24 \times 10^{53}$	3664	1.98	85.2	0.0452	6.8	$1.24 \times 10^{53}$
3745	2.21	84.3	0.0430	5.9	$1.05 \times 10^{53}$	3765	25.29	72.6	0.0357	1.4	$5.62 \times 10^{52}$
3788	5.20	65.7	0.0187	1.1	$6.44 \times 10^{51}$	3843	2.33	50.5	0.0179	1.5	$5.54 \times 10^{51}$
3853	3.08	91.3	0.1850	12.0	$1.39 \times 10^{55}$	3860	4.44	31.5	0.0168	1.0	$4.47 \times 10^{51}$
3879	1.51	30.9	0.0407	6.5	$8.70 \times 10^{52}$	3891	13.69	41.5	0.0305	1.5	$3.32 \times 10^{52}$
3893	3.70	35.7	0.0109	0.6	$1.05 \times 10^{51}$	3900	1.53	86.7	0.0682	12.0	$4.93 \times 10^{53}$
3905	4.39	24.3	0.0359	3.1	$5.71 \times 10^{52}$	3906	2.32	20.7	0.0218	2.0	$1.07 \times 10^{52}$
3912	4.04	26.0	0.0376	3.5	$6.69 \times 10^{52}$	3918	2.00	110.5	0.0249	2.6	$1.67 \times 10^{52}$
3929	3.97	28.5	0.0197	1.3	$7.71 \times 10^{51}$	3954	8.19	29.7	0.0472	3.6	$1.44 \times 10^{53}$
4039	5.45	58.8	0.0278	1.9	$2.45 \times 10^{52}$	4157	2.27	20.0	0.0130	0.9	$1.91 \times 10^{51}$
4216	1.51	25.5	0.0347	5.0	$5.14 \times 10^{52}$	4350	3.27	52.0	0.0418	4.6	$9.55 \times 10^{52}$
4368	56.23	36.5	0.0183	0.4	$6.04 \times 10^{51}$	4701	7.14	74.7	0.0400	3.0	$8.26 \times 10^{52}$
5304	13.28	22.8	0.0166	0.6	$4.34 \times 10^{51}$	5389	4.14	23.7	0.0406	4.0	$8.68 \times 10^{52}$
5419	3.43	22.8	0.0211	1.6	$9.65 \times 10^{51}$	5421	1.97	266.8	0.0536	9.2	$2.20 \times 10^{53}$
5433	2.83	76.0	0.1560	12.0	$7.87 \times 10^{54}$	5447	3.88	55.9	0.0299	2.5	$3.10 \times 10^{52}$
5450	4.15	172.2	0.0712	10.3	$5.69 \times 10^{53}$	5451	4.30	24.5	0.0226	1.6	$1.21 \times 10^{52}$
5464	2.60	28.9	0.0382	4.5	$7.07 \times 10^{52}$	5470	4.79	30.4	0.0677	8.7	$4.80 \times 10^{53}$
5472	1.96	55.1	0.0371	4.9	$6.43 \times 10^{52}$	5473	3.79	80.6	0.0554	6.9	$2.46 \times 10^{53}$
5475	2.42	72.8	0.0552	8.7	$2.43 \times 10^{53}$	5476	2.55	21.9	0.0331	3.6	$4.39 \times 10^{52}$
5478	2.96	297.0	0.0688	11.6	$5.08 \times 10^{53}$	5479	2.76	137.3	0.0476	6.3	$1.47 \times 10^{53}$
5484	2.68	64.6	0.0656	11.2	$4.32 \times 10^{53}$	5486	9.35	86.7	0.0354	2.2	$5.48 \times 10^{52}$
5489	9.44	140.5	0.0470	3.4	$1.41 \times 10^{53}$	5495	2.12	26.3	0.0701	12.0	$5.39 \times 10^{53}$
5518	2.35	51.9	0.0531	8.3	$2.13 \times 10^{53}$	5526	3.38	72.4	0.0281	2.4	$2.54 \times 10^{52}$
5531	1.67	33.9	0.0124	1.0	$1.62 \times 10^{51}$	5539	1.88	77.8	0.1066	12.0	$2.20 \times 10^{54}$
5541	1.66	26.4	0.0349	4.8	$5.24 \times 10^{52}$	5548	5.95	187.8	0.0384	3.0	$7.16 \times 10^{52}$

<sup>1</sup> Electronic version of table available from efenimore@lanl.gov

Fig. 1.— Luminosity and variability for BATSE bursts with known redshifts. The six bursts are labeled by the BATSE trigger numbers (see Table 1). The two solid lines bound the region that contains the average of the distribution. Many more bursts will be necessary to define the average of this distribution more accurately.

Fig. 2.— Luminosity and variability for BATSE bursts including GRB980425 (BATSE trigger number 6707). If GRB980425 is associated with SN 1998bw, it is very close ( $z = 0.0085$ ) and much less luminous than other GRBs. The association is controversial (Galama et al. 1999b, Woolsey et al. 1999, Kulkarni et al. 1998, Graziani, Lamb, & Masion 2000). GRB980425 has the lowest observed variability, which is in general agreement with our proposed trend.

Fig. 3.— Comparison of variability from this paper and that of Reichart et al. 2000. Although defined somewhat differently, the two definitions are highly correlated.

Fig. 4.— Luminosities and redshifts from variability for 220 long and bright BATSE GRBs. The six solid squares are the GRBs with known redshifts (excluding GRB980425, see Table 1) that were used to calibrate the luminosity – variability relationship. Bursts with  $z > 12$  were placed at  $z = 12$ . The solid curves are lines of constant peak flux ( $\text{photon cm}^{-2} \text{s}^{-1}$ ). The lower edge of the envelope of events is due to our selection criteria that  $P > 1.5 \text{ photon cm}^{-2} \text{s}^{-1}$ . Previous studies only knew the number of GRBs between sets of solid curves and not their distribution in luminosity and redshift. The projection of the distribution onto the luminosity axis would give the GRB luminosity function and the projection onto the redshift axis would give the progenitor rate if both were unaffected by the BATSE threshold.

Fig. 5.— Luminosities and redshifts from variability for 220 long and bright BATSE organized into ranges of redshifts and luminosities. The dotted lines bracket seven regions of the luminosity – redshift space defined by ranges of  $z$  and where the luminosity function within the range is unaffected by the threshold. The solid lines bracket nine regions of the luminosity – redshift space defined by ranges of luminosity where the GRB formation rate within the range is unaffected by the threshold.

Fig. 6.— The number distribution of GRBs for seven ranges of  $z$ , assuming bursts occur at a constant rate per time-volume. In each range, we present the number distribution ( $\text{Log } N - \text{Log } L_{256}$ ) down to the luminosity at which that range is complete. The seven ranges (labeled 1 to 7) are from Figure 5 and are bounded by  $z = 0.3, 0.75, 1.25, 2.0, 3.0, 5.0, 7.0, \text{ and } 10.0$ . All ranges of  $z$  should have the same number distribution, but this is clearly not the case. We conclude that bursts do not occur at a constant rate per time-volume.

Fig. 7.— The number distribution of GRBs for seven ranges of  $z$  assuming bursts occur at a rate per time-volume that is proportional to the SFR of Steidel et al. 1999. In each range, we present the number distribution ( $\text{Log } N - \text{Log } L_{256}$ ) relative to the amount of star formation down to the luminosity at which that range is complete. The  $z$  ranges are the same as in Figure 6. All ranges of  $z$  do not fall on a common curve indicating that the assumption that the burst formation

rate follows the star formation rate is invalid. We conclude there must be relatively more burst formation than star formation at high  $z$ .

Fig. 8.— The number distribution of GRBs for seven ranges of  $z$  shifted so that they all fall on a common curve. The  $z$ -ranges are the same as in Figure 6. The amount of shifting relative to Figure 6 gives the relative burst formation rate.

Fig. 9.— The relative GRB formation rate and SFR. The histogram (with squares) is the GRB formation rate needed to shift the Log  $N$ –Log  $L_{256}$  distributions in Figure 6 to agree with Figure 8. The error bars represent the statistical uncertainty on each point. This histogram is the burst formation rate determined solely from gamma-ray data without assuming a luminosity function or a dependency on a SFR. The dotted histograms are based on the two power laws in Figure 1 (also see eqs. [6,7]) and they represent the systematic uncertainty in our burst formation rate. The solid curve is the SFR based on the observations listed by Steidel et al. 1999. The dotted curve is from the dust-corrected SFR from observations listed by Blain & Natarajan 1999. The SFRs are normalized to the GRB formation rate at  $z = 1$ . The GRB formation rate scales approximately as  $(1 + z)^{3.3 \pm 0.3}$ . The formation rate for GRBs continues to rise for  $1 + z > 2$  whereas the star formation observations indicates that the rate levels off or decreases. The dotted line is a theoretical estimate of the star formation rate at high  $z$  (from Gnedin & Ostriker 1997).

Fig. 10.— The GRB luminosity function. The BATSE threshold prevents us from seeing all GRBs in a particular luminosity band. BATSE, at a particular luminosity, is complete to a redshift  $z_c$ . We correct the observed number of events from redshifts less than  $z_c$  to the total number that would be seen to  $z = \infty$ . The solid line assumes that the number of GRBs is proportional to the SFR of Steidel et al. 1999. The dotted line uses the GRB formation rate from Figure 9 and, thus, is completely derived from gamma-ray data without any assumptions of star formation rate nor a form for the GRB luminosity function. The GRB luminosity rolls over at low luminosity, and is a power law above  $4 \times 10^{51}$  erg s $^{-1}$  with an index of  $\sim -1.9$  if based on the SFR and  $\sim -2.3$  if based on the GRB formation rate.

Fig. 11.— The aligned peak test for the first six ranges of  $z$  in Figure 5. The order of the curves (from low to high  $z$ ) is solid, dotted, dashed, dot-dashed, dot-dot-dashed, and long dashed. The largest peak in each GRB within each range of  $z$  was aligned and averaged to give the average peak shape. Peaks from lower  $z$ 's should be wider due to time dilation. All ranges give about the same width, an effect which might be due to the small number of bursts available.

Fig. 12.— The aligned peak test for the first six ranges of  $z$  in Figure 5, corrected for time dilation. The curve definitions are the same as in Figure 11. The time history of each burst was stretched by the expected time dilation based on the  $z$  estimated from variability (from Table 2). Thus, all ranges of  $z$  should give the same peak width. In fact, the dispersion appears to be larger than in Figure 11, indicating that this test may not support the idea that variability can give valid redshifts. However, the small number of GRBs and limited range of  $z$  weakens this test (see text).

Figure 1

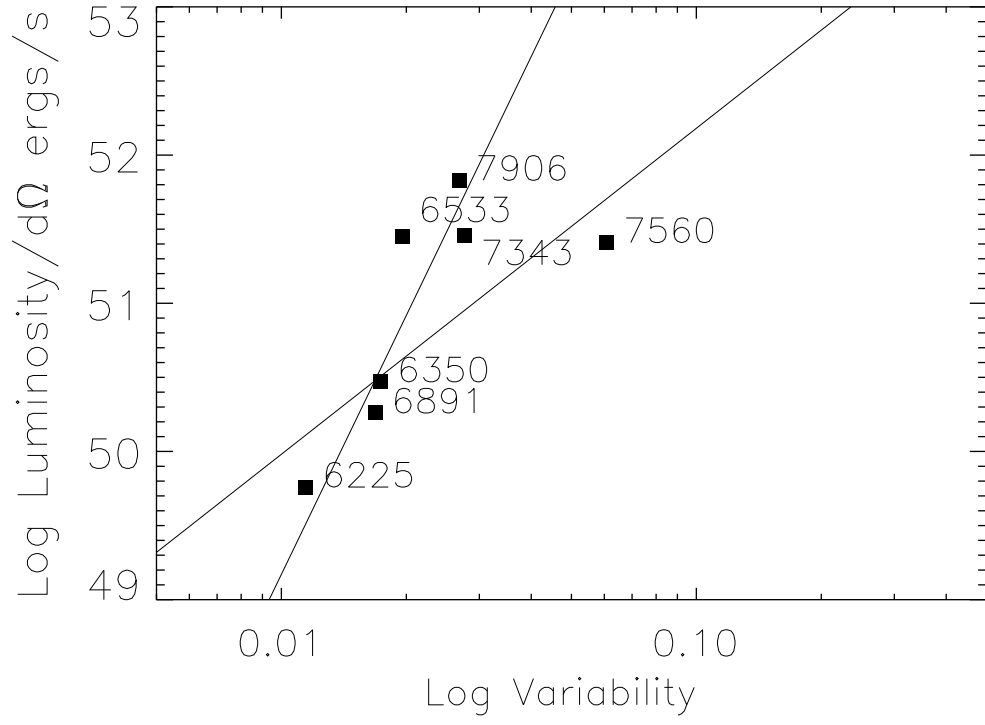


Figure 2

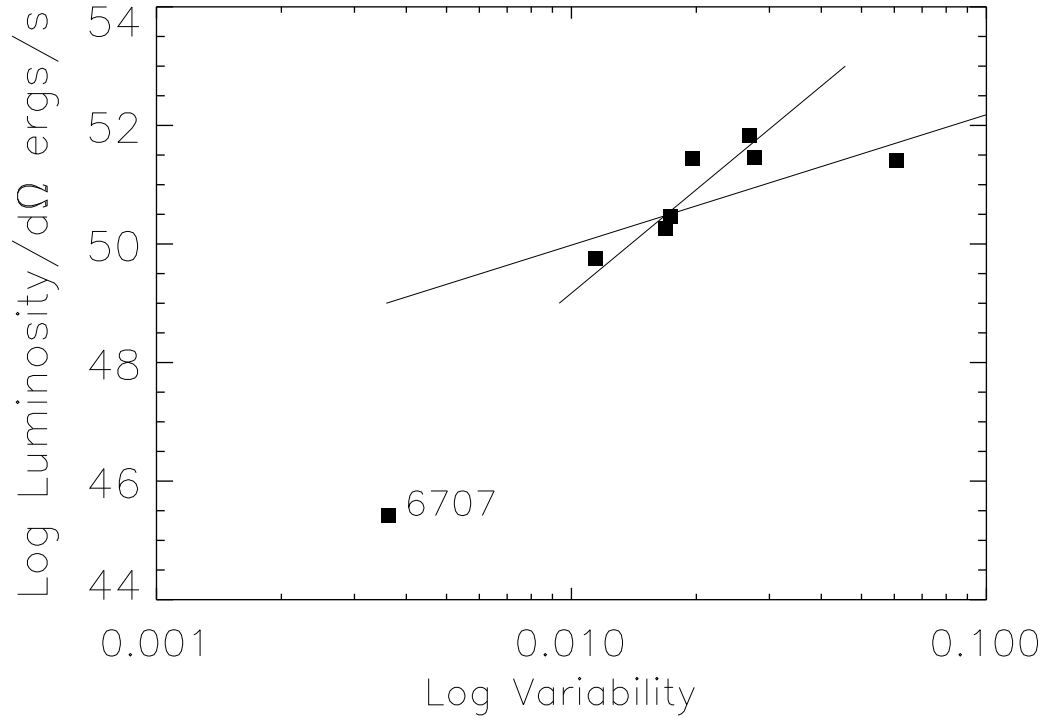


Figure 3

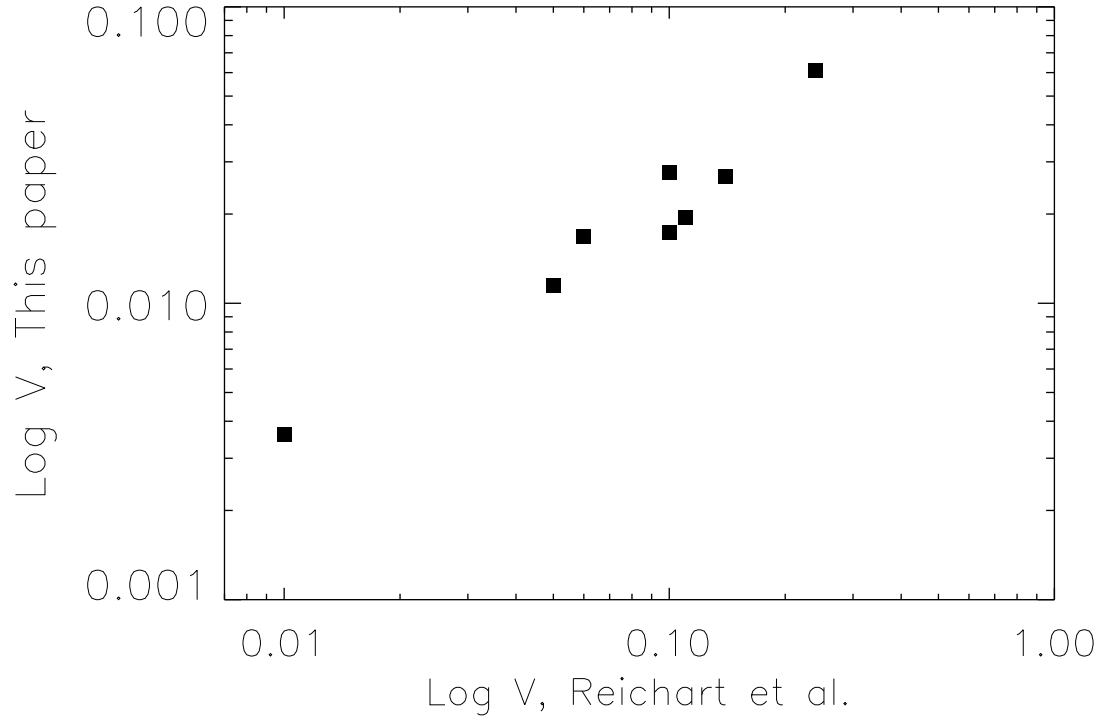


Figure 4

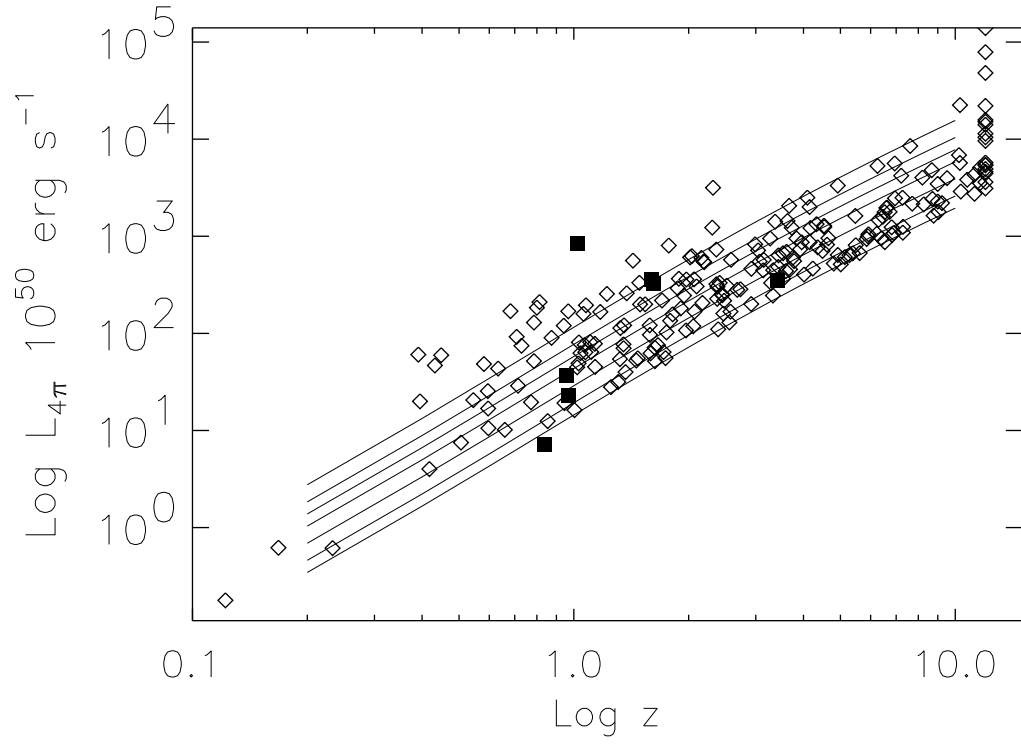


Figure 5

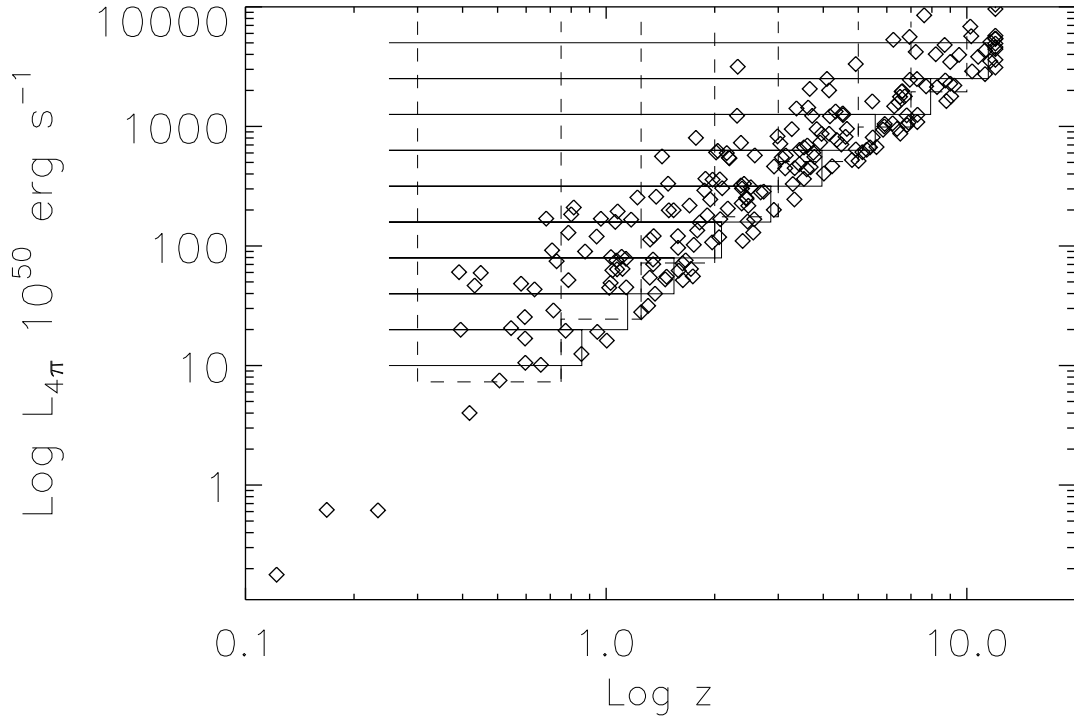


Figure 6

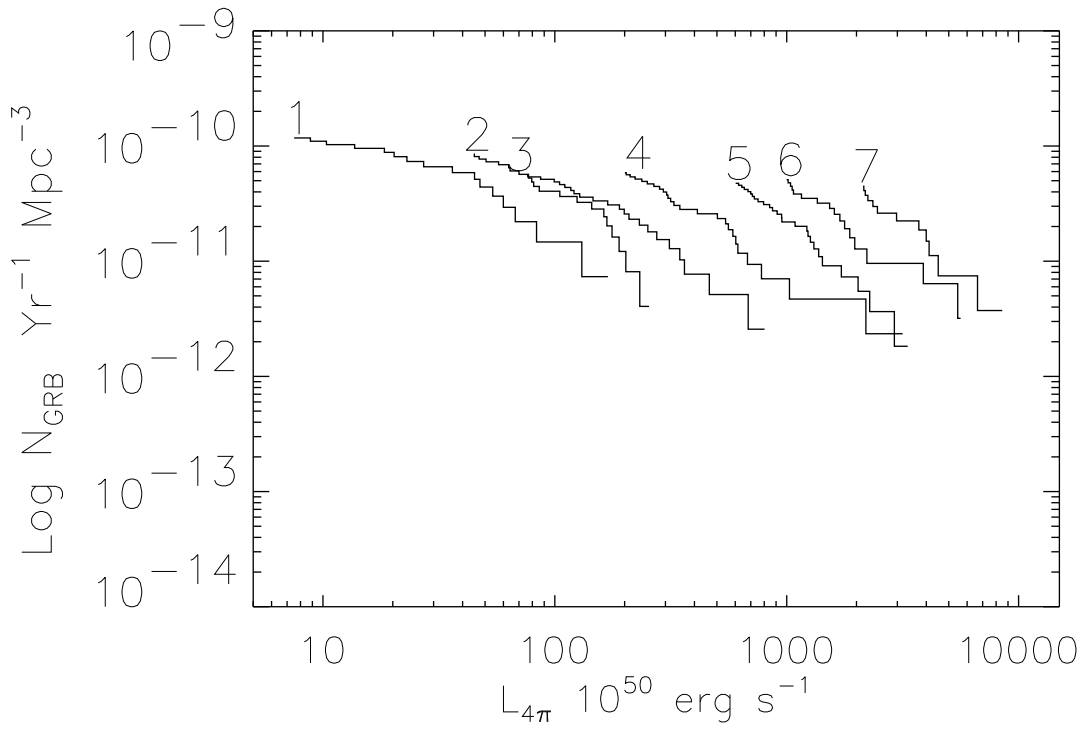


Figure 7

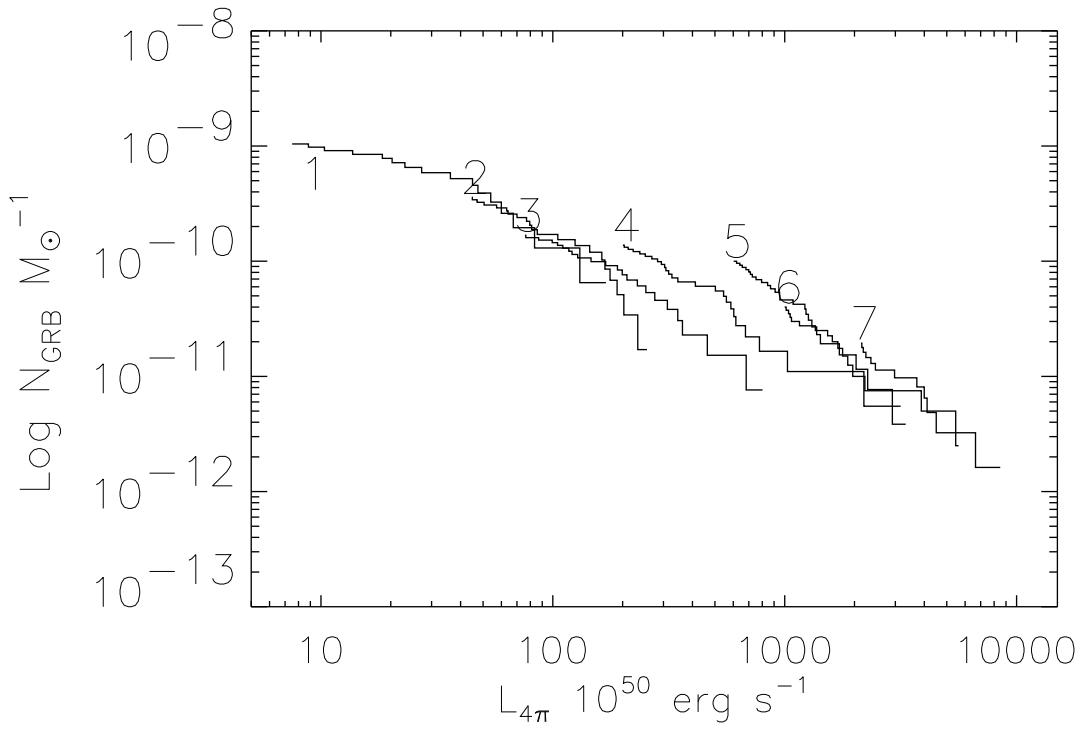


Figure 8

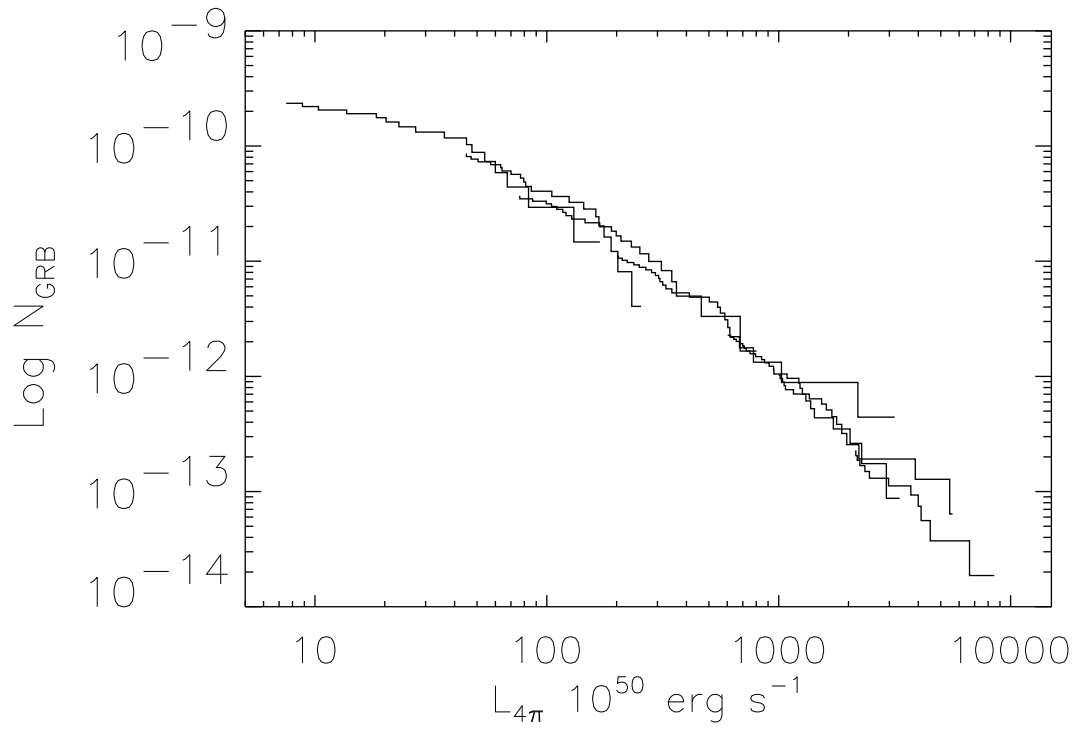


Figure 9

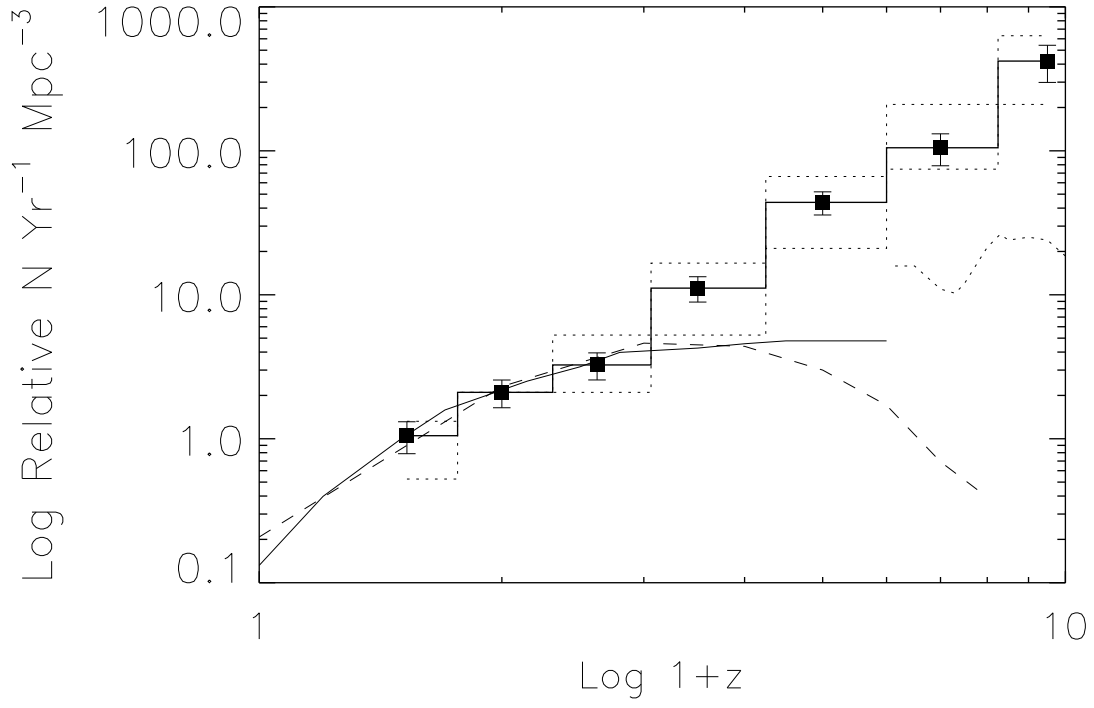


Figure 10

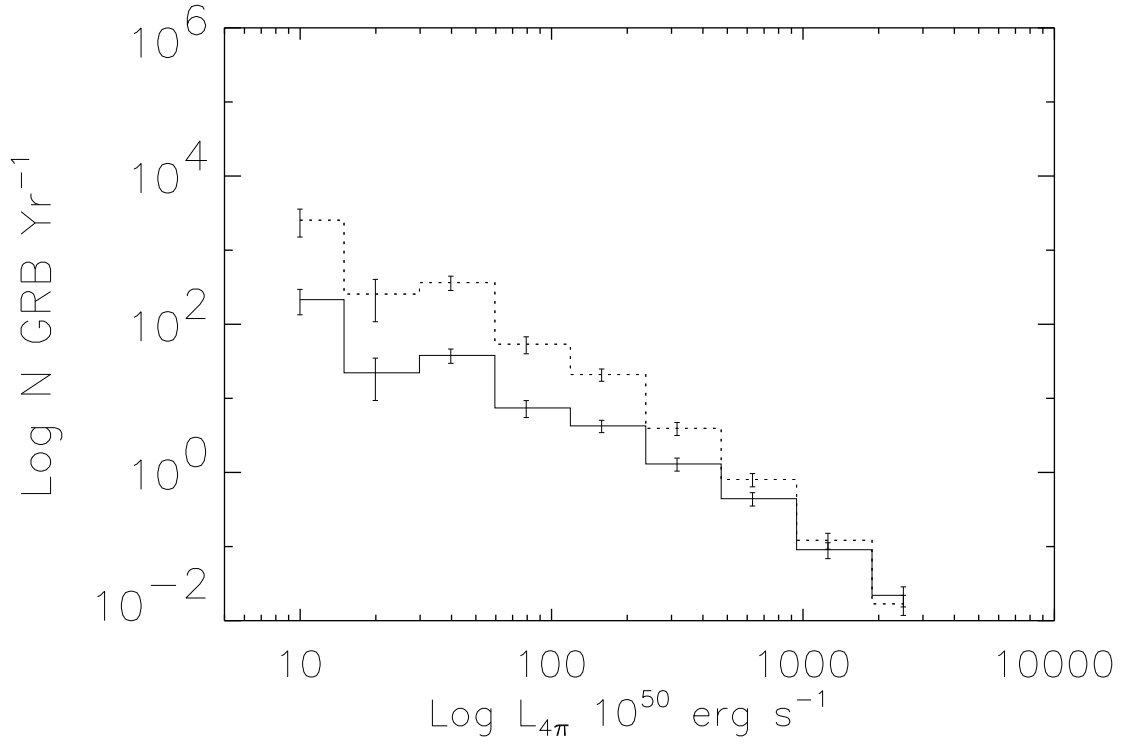


Figure 11

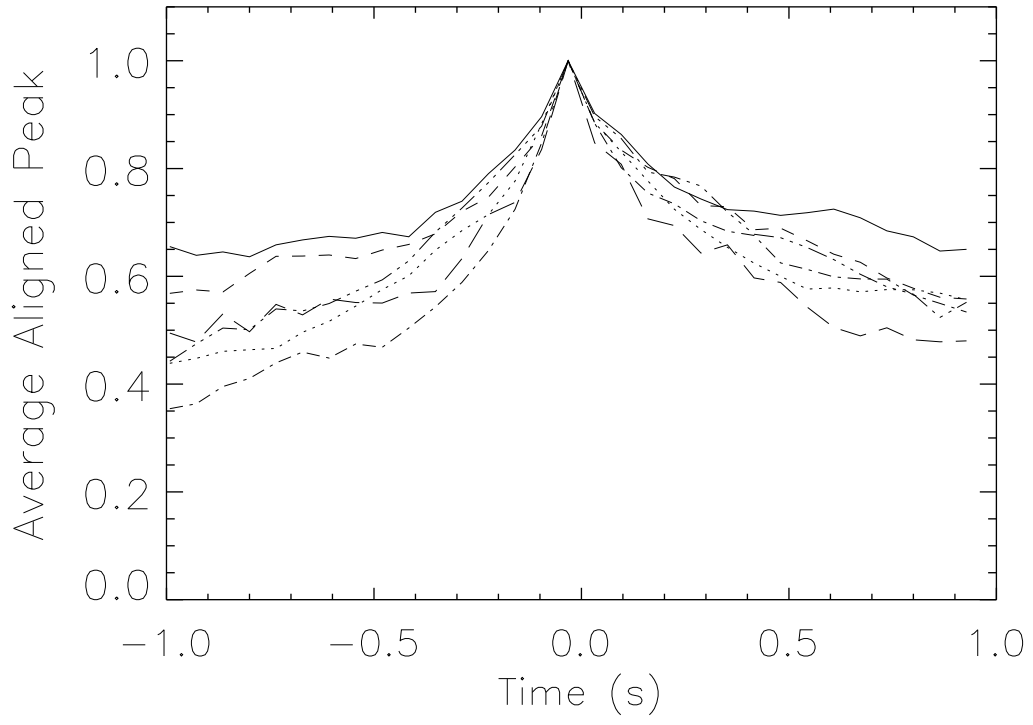


Figure 12

